REVISTA MATÉRIA
V.23 N.02
ISSN 1517-7076 artigo e-11998, 2018

Electrochemical corrosion characterization of nickel aluminides in acid rain

Engelbert Huape Padilla [1], Ariosto Medina Flores [2], Claudio Aguilar Ramírez [3]
Ismeli Alfonso López [4], Luis Béjar Gómez [1]

[1] Facultad de Ingeniería Mecánica, Universidad Michoacana de San Nicolás de Hidalgo. Santiago Tapia 403, Col. Centro, CP: 58000, Morelia, Michoacán, México.
e-mail: pahuen@gmail.com, lbejargomez@yahoo.com.mx
[2] Instituto de Investigación en Metaúrgia y Materiales, Universidad Michoacana de San Nicolás de Hidalgo. Santiago Tapia 403, Col. Centro, CP: 58000, Morelia, Michoacán, México.
[3] Instituto de Investigaciones en Materiales Universidad Nacional Autónoma de México, Unidad Morelia. Antigua Carretera a Pátzcuaro No. 8701 Col. Ex-Hacienda de San José de la Huerta. CP: 58190, Morelia, Michoacán, México.
[4] Departamento de Ingeniería Metalúrgica y de Materiales, Universidad Técnica Federico Santa Maria. Av. España 1680, Valparaíso, Valparaíso, Chile.
e-mail: ariosto@umich.mx, claudio.aguilar@usm.cl, ialfonso@unam.mx

ABSTRACT

Nickel aluminides have been extensively studied in recent decades to replace superalloys, in some components of aircraft turbines, because they have excellent corrosion resistance. Many industrial cities have the problem of air pollution, which has forced the study of the degradation of these alloys in the presence of acid rain. The aim of this work is to study the electrochemical corrosion behavior of nickel aluminides in a medium of simulated acid rain. Potentiodynamic Polarization, Linear polarization resistance curves, Rp, Nyquist data and Bode curves obtained by electrochemical impedance spectroscopy were used to study the corrosion behavior of two intermetallic compounds. The polarization curves show that both intermetallic Ni_3Al and NiAl have very similar corrosion potential, showing a slightly nobler behavior the NiAl intermetallic. The intermetallic Ni_3Al has an active-passive behavior where the anode branch presents a general dissolution of the alloy, indicating that it is under cathodic control. NiAl intermetallic shows an active dissolution region, followed by a passive behavior. At longer immersion times, Ni_3Al intermetallic has a higher polarization resistance, which means a lower corrosion rate.

Keywords: Nickel Aluminides, Electrochemical impedance spectroscoy, Acid Rain, Nanoindentation.

1. INTRODUCTION

Nickel aluminides such as NiAl and Ni_3Al have received considerable attention for high temperature structural and coating applications in aerospace field [1-3], and due to high temperature strength, high corrosion resistance, high thermal and electrical conductivity, high melting temperature (1638°C), high Young's module (240GPa) have been regarded as a promising candidate for the high temperature applications [4,5]. Ni-base superalloys, Co alloys and steels are widely used in applications such as aircraft turbine blades and power plants due to present good corrosion resistance at elevated temperatures, however, the lower density (5.86g/cm^3) than superalloys and excellent high temperature oxidation resistance, allowed nickel aluminides being extensively studied in the past decades to replace superalloys [6-8]. As the nickel aluminides also has good properties for low temperature applications, studies of corrosion resistance at low temperature in aqueous media is interesting, because these materials will not always be at the operating temperatures, and corrosion damage during manufacture or maintenance may result in catastrophic failure during service [9].

Nickel aluminides have excellent corrosion resistance in most environments, accordingly, are being used as biomedical metallic materials to replace alloys such as stainless steel, most of the used materials for human implants include. NiAl intermetallics compounds have been investigated by electrochemical

Corresponding Author : Engelbert Huape Padilla Received on: 01/08/2017 Accepted on: 04/09/2017

10.1590/S1517-707620180002.0335

experiment in Hank's solutions [10]. Trinstancho *et al*. investigated the possible mechanism controlling the rate of the corrosion processes in hot corrosion resistance of Inconel 718 from 588°C to 900°C in Na_2SO_4, $80V_2O_5$-$20Na_2SO_4$, $NaVO_3$ and natural ash [11].

Acidic deposition in some areas of the world has received increasing interest in the raising emission of SO_2 and NO_x. This can be attributed to the accelerated rate of economic development [12]. The acid rain is primarily caused by the precursors of strong acids such as H_2SO_4 and HNO_3, resulted from fossil fuel combustion [13]. pH values vary depending upon country as well as the area, for example, on the south-western coast of Europe, the pH values of samples collected fluctuating from 4.48 to 6.88 [14]. In 2008, China reported high acidity in rain water, the pH value of rain sample was 3.7 [13]. Nickel aluminides are prone to be attacked in atmospheric corrosion in urban and coastal areas, industrial and marine environments corrosion are more aggressive due to the highly corrosive nature of air pollutants [15]. Electrochemical impedance spectroscopy (EIS) is a technique which has been widely used in the study of aqueous corrosion and has proved effective in determining and understanding reaction mechanism and kinetics of corrosion processes.

The purpose of the present research work is to evaluate the corrosion behaviors of Ni_3Al and NiAl alloys in simulated acid rain by using the electrochemical techniques to establish the involved mechanism in the process.

2. MATERIALS AND METHODS

2.1 Materials

Cast ingots of binary NiAl (Table 1) were produced as round 20 g buttons with 99.99% pure Al, 99.97% pure Ni, on a water-cooled copper crucible under an Ar atmosphere. The buttons were remelted at least 8 times to ensure sufficient homogeneity. Ingots were cooled inside the crucibles in the furnace at room temperature and in this condition were used. Chemical composition was determined by SEM-EDX (field emission, JSM-7401F). The phase composition of the alloys was determined by the XRD method with a PANalytical diffractometer using CuKα radiation. The data identification was carried out using the Match software.

Table 1: Chemical composition of the tested alloys.

SAMPLES	ALLOY COMPOSITION			
	(wt.%)		(at.%)	
	Ni	Al	Ni	Al
NiAl	69.94	30.06	51.68	48.32
Ni_3Al	86.93	13.07	75.35	24.65

2.2 Sample preparation

The test specimens were cut into small parallelepiped pieces using a diamond tipped blade. Subsequently, the samples were encapsulated in fast cure acrylic which, in turn, were performed by grinding the specimens from 180 to 4000 grit paper for mechanical properties measurement by nanoindentation technique. For electrical connection, specimens were spot-welded to a wire, then were encapsulated in fast cure acrylic. Sample surfaces were ground to 1000 grade grit paper and then rinsed with ethanol in an ultrasonic bath for 20 minutes. Specimens with this surface condition were employed as the working electrode (we) in the electrochemical tests.

2.3 Mechanical properties by Nanoindentation technique

Nanoindentation measurements were performed in the polished surface of the samples with a matrix array 4 by 4 to determine the mechanical properties such as hardness and Young's modulus. The nanoindentation tests were carried out by an Agilent Nano Indenter G200, with a Berkovich diamond indenter with radius of 20 nm and maximum load of 5 mN. The equipment was calibrated using a standard fused silica sample, following the method described elsewhere [16]. Tests parameters as the constants of area function were C0=24.08, C1= -179.336, C2= 6721.28, C3= -24409.2, and C5= 18691.8. The analysis of the load displacement curve was carried out by Oliver and Pharr method [17]. Residual indentation of samples was recorded by the AFM NanoVision system attached to the nanoindenter system.

2.4 Electrochemical techniques

In order to simulate the acid rain conditions, the chemical composition for the environment for in vitro corrosion studies at pH 2.3, is given in Table 2. It was prepared with distilled water and analytical grade reagents following previously-reported concentrations [18].

Electrochemical tests were performed using an ACM Instruments potentiostat controlled by a computer. All potentials were measured using a Saturated Calomel Electrode (SCE) as reference electrode and a graphite bar counter electrode. All tests were performed at 19°C. The volume of electrolytic solution into the cell was 60 ml. The electrochemical techniques included potentiodynamic polarization curves, linear polarization resistance (LPR) and electrochemical impedance spectroscopy (EIS) measurements. Corrosion rates were calculated in terms of the corrosion current, I_{corr}, by using linear polarization resistance curves.

Potentiodynamic polarization curves were obtained by varying the applied potential with respect to the open circuit potential (OCP), from -1500 mV up to +1500 mV at a scan rate of 1 mV/s in according with ASTM G3-89. A delay time of 60 min was setup until a stable reading was achieved, after that, electrochemical tests started. EIS tests were carried out by using a signal with amplitude of 20 mV (RMS) *vs*. the OCP between a frequency interval of 0.05 Hz to 10 kHz obtaining a measurement at 30 min, 12 and 24 hours of immersion and the number of points per frequency decade was 9. Measurements of LPR were performed by polarizing the specimen from +15 to -15 mV *vs*. OCP at a scan rate of 1 mV/s each 15 minutes during 24 hours. Corrosion products analysis of as-cast corroded samples was performed by scanning electron microscope (SEM) and energy X-ray dispersive spectroscopy (EDS).

Table 2: Concentrations of simulated acid rain solution.

COMPONENT	CONCENTRATION
Sulphuric acid	0.06 $ml \cdot L^{-1}$
Nitric acid	0.02 $ml \cdot L^{-1}$
Sodium nitrate	0.0265 $g \cdot L^{-1}$
Ammonium sulfate	0.0462 $g \cdot L^{-1}$
Sodium sulfate	0.0345 $g \cdot L^{-1}$
Sodium chloride	0.0875 $g \cdot L^{-1}$

3. RESULTS

3.1 Microestructural characterization

The as-cast microstructures of the Ni_3Al and NiAl alloys are shown in Fig. 1a and 1b, respectively. As show in Fig.1a, Ni_3Al alloy has a dendritic morphology with a grain size bigger than 300 μm with the presence of pores; higher Ni contents and high cooling rates induce dendrite formation [1]. No precipitates were observed in this intermetallic alloy, confirmed by X-ray diffraction pattern, where crystal structure corresponding to Ni_3Al alloy and no second phases were detected, see Fig. 2a. In Fig. 1b, NiAl alloy is composed of elongated and equiaxed grains with average size around 500-700 μm, with the presence of pores. X-ray diffraction pattern of NiAl intermetallic alloy confirmed the crystal structure corresponding to NiAl without the presence of second phases and precipitates, as can be seen in Fig. 2b.

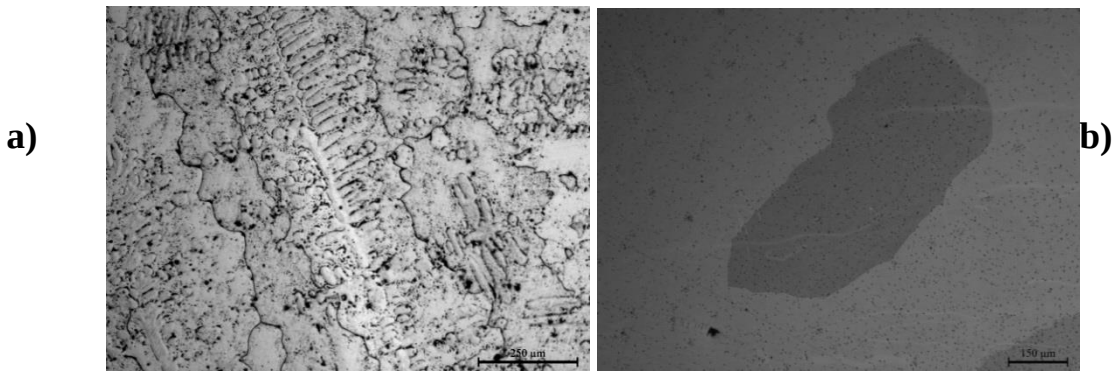

Figure 1: Micrograph of the as-received state sample a) Ni_3Al and b) NiAl.

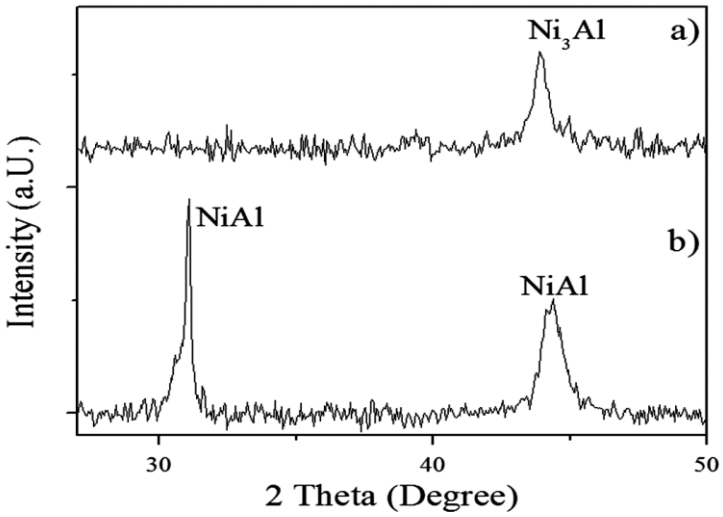

Figure 2: X-ray diffraction patterns of the as-cast condition sample of a) Ni_3Al and b) NiAl system alloys.

Figure 3a shows the load-displacement curves for the samples Ni_3Al and NiAl and both of them provides a good repeatability for the sixteen indentations applied. The values of elastic modulus and hardness obtained are present in Table 3, where this behavior agrees with that reported by DONGMIN SHI *et al*. [19]. In the notch tip Berkovich, upon unloading from a maximum load of 5 mN there are no irregularities in size, shape or cracking, as show in the AFM image of Fig. 3b.

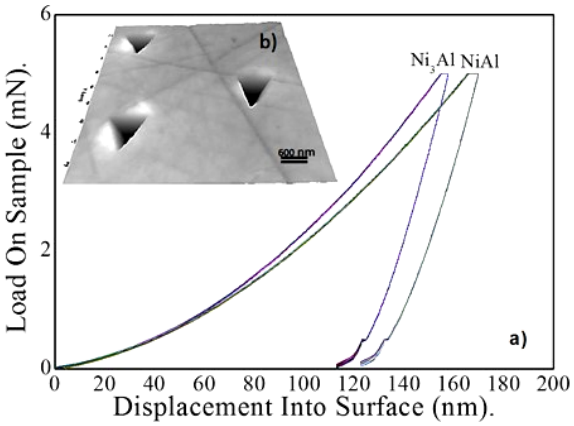

Figure 3: a) Load-displacement curves of both samples NiAl and Ni_3Al by Nanoindentation technique, and b) AFM image show Berkovich tip residual impression areas.

Table 3: Results of Elastic Modulus and hardness evaluated with Berkovich tip.

SAMPLES	YOUNG'S MODULUS (GPa)	HARDNESS (GPA)
NiAl	261.98±8.9	9.88±0.3
Ni_3Al	204.67±14.5	9.31±1

3.2 Potentiodynamic Polarization Curves

Polarization curves for the system NiAl are shown in Figure 4. The results show that both intermetalics have very similar corrosion potentials, being observed a slightly nobler behavior for the NiAl intermetallic. The polarization curve for Ni_3Al alloys present a dissolution continuously behavior where the anodic branch presents a general dissolution of the alloy, indicating that it is under cathodic control. NiAl alloy shows an active region of dissolution in a range of potential from -320 to -160 mV/SCE, followed by passive behavior in the range of -116 mV to -24 mV/SCE. During the increase of the overpotential around 32 mV/SCE, presents a semi-passive behavior and current limit with fluctuations of density over a range of 104 mV/SCE, approximately, where are presents a pitting potential similar to observed in a NiAl intermetallic [20].

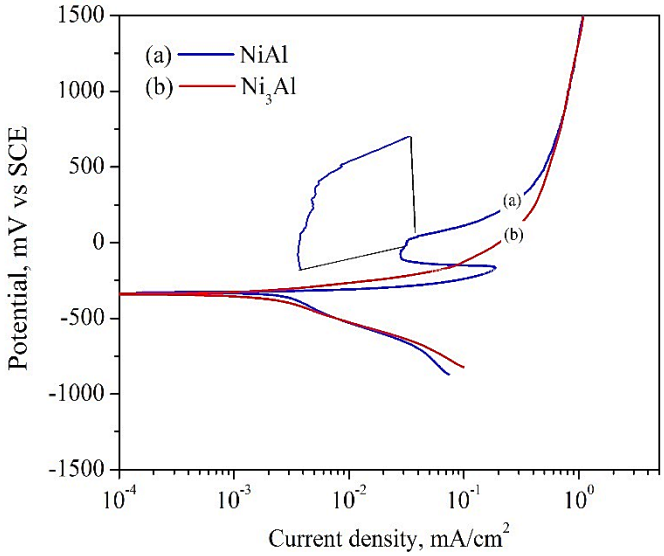

Figure 4: Potentiodynamic polarization plots of Ni_3Al and NiAl as-cast condition in acid rain electrolyte at 1 mV/s.

The values of corrosion potential (E_{corr}) and corrosion current density (i_{corr}) obtained by the method of intercepts are showed in table 3. The Tafel slopes were determined by a linear array of the polarization data in the range of ±150mV of the E_{corr}, can be observed in the intermetallic Ni_3Al, in the beginning the reaction rate is relatively slow in the cathodic slope, where the reactants are abundant and the reaction products move easily, being controlled by an activation process. When a so great negative potential is applied in an acid medium, the activation energy is given by the reduction of cathodic hydrogen on the sample surface, this gaseous hydrogen formation causes the H^+ concentration decrease, increasing the local pH value.

Table 4: Electrochemical parameters obtained from polarization plots.

SAMPLES	β_a (mV/decade)	β_c (mV/decade)	E_{corr} (mV//SCE)	E_{pit} (mV/SCE)	i_{corr} (mA/cm^2)
NiAl	27	115	-326,77	-62.5	0,00151
Ni_3Al	17	27	-339,21	----	0,000540

3.3 Long term tests

Figure 5 shows the results of the variation of corrosion potential, E_{corr}, with respect to time. Ni_3Al intermetallic presents an increase of the value of E_{corr} within the first 2 hours from -400mV to -338 mV/SCE, subsequently, stabilized in the latter value. Similarly, the NiAl intermetallic presents a gradual increase of E_{corr} in a range from -355 mV to -229 mV/SCE during the first 2.4 hours approximately, showing a fluctuation between 4 and 8 hours. Subsequently, E_{corr} values are stabilized for both intermetallic, which is related to a more homogeneous form of corrosion including the surface of the localized corrosion sites [9]. The interaction between the surface and Cl^- leads to change of E_{corr} to more negative values [21], as observed for the Ni_3Al intermetallic.

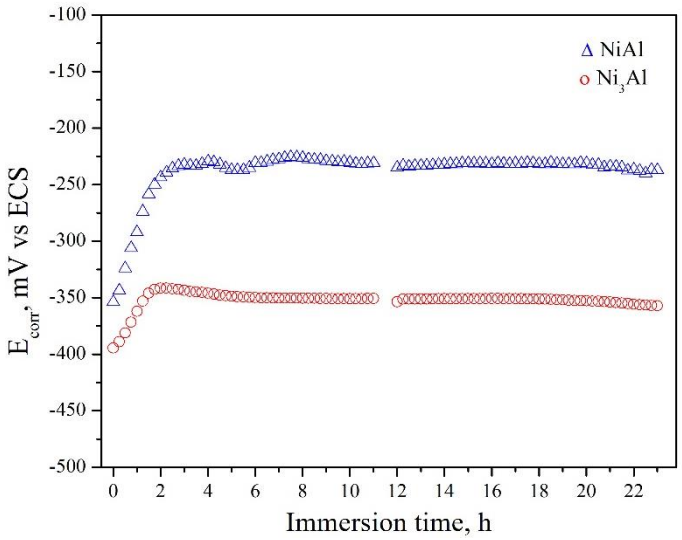

Figure 5: Ecorr diagram of Ni_3Al and NiAl Intermetallics alloys in acid rain electrolyte at 1 mV/s.

Figure 6b shows the images of the corroded surfaces of NiAl intermetallic, where pitting corrosion sites are seen and caused by the presence of NaCl [2]. The presence of corrosion products onto the metallic surfaces was not observed, indicating that they were soluble and dissolved during the washing step of the working electrodes. Ni surface did not show a significant attack, since the presence of lines generated by the grinding process is still seen. In Figure 6a, it can be seen that the dissolution of the metal in the corrosion process of Ni_3Al occurs preferentially in the interdendritic regions.

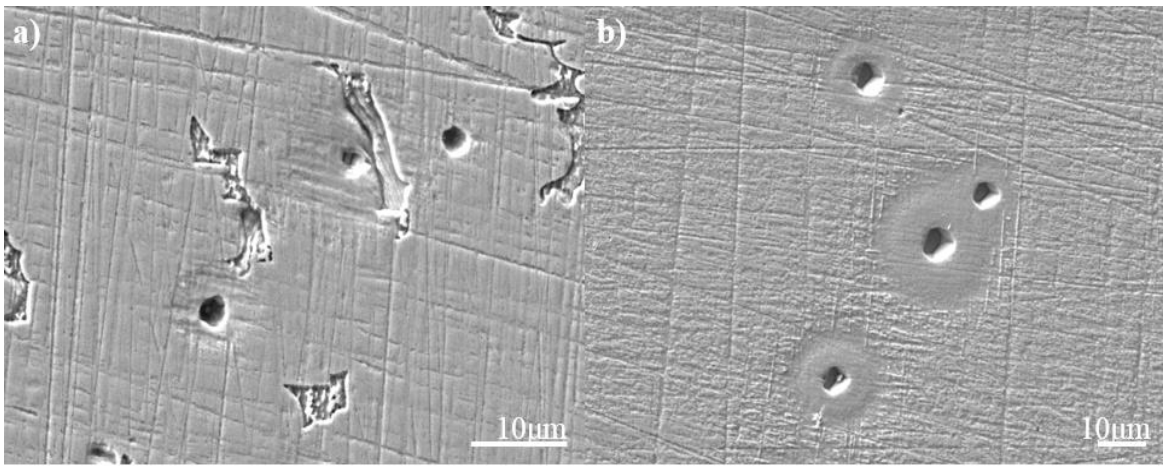

Figure 6: SEM micrograph of the corroded surfaces in simulated acid rain as cast condition of a) Ni_3Al and b) NiAl.

From the results of linear polarization (LPR) resistance, the corrosion rate of kinetics was calculated (see Figure 7) according to the standard ASTM G102, where the corrosion rate is expressed by equation 1:

$$CR = k\frac{i_{corr}}{\rho}EW \quad (1$$

Where EW is the equivalent weight of the alloy, i_{corr} is the corrosion current density, ρ = density of the alloy, and K = constant. The equivalent weight was calculated with equations 2 and 3.

$$EW = \frac{1}{Q} \quad (2$$

$$Q = \sum \frac{n_i f_i}{W_i} \quad (3$$

Where f_i = the fraction of mass of the element i-th in the alloy, W_i = atomic weight of the i-th element in the alloy and n_i = the valence of the i-th element of the alloy.

The corrosion current density was calculated from measurements of the polarization resistance, as follows:

$$i_{corr} = \frac{B}{Rp} \quad (4$$

Where B = constant Stern-Geary, which was obtained with the anodic (β_a) and cathodic (β_c) Tafel slopes, with the following equation:

$$B = \frac{\beta_a \beta_c}{2.303(\beta_a + \beta_c)} \quad (5$$

The kinetics of the corrosion rate of both alloys of the NiAl system is shown in Figure 7, obtained from LPR measurements. The results show that during the first 2 hours the values of the corrosion rate of the intermetallic Ni_3Al decrease from 3.8 to 1.5 µm/year, remaining constant at this value. On the other hand, the NiAl intermetallic presents a decrease of 9.7 to 3 µm/year, with CR fluctuations in the first 12 hours, a slight decrease occurs for the remainder of the test with a tendency to estabilize from this time. The Ni_3Al intermetallic has a lower corrosion rate. This behavior of the CR is an effect caused by the sulfuric acid in the corrosion rate of the base Ni intermetallic [2].

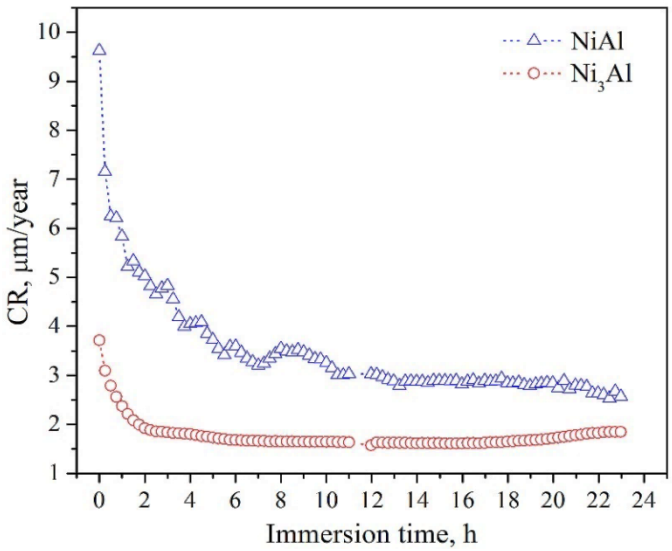

Figure 7: Corrosion rate kinetics of corroded Ni-Al intermetallics immersed in simulated acid rain solution.

3.4 Electrochemical Impedance Spectroscopy

Figures 8 and 9 show the impedance behavior of the Ni_3Al and NiAl intermetallics in the acid rain solution

and both alloys exhibit capacitive behavior at middle frequencies, increasing in magnitude with the immersion time. In the first 30 minutes of immersion, both alloys have diminished semicircles close to high frequencies associated to the activation behavior followed by a resistive behavior in Ni_3Al and inductive for NiAl (figures 8a and 9a) associated with localized corrosion [22]. EIS results show, at 12 and 24 hours of immersion, a modification in the final behavior for both alloys. In this sense, EIS results for Ni_3Al at 12 hours of immersion showed a resistive behavior followed by a capacitive behavior at high and middle frequencies, respectively, the latter describing a loop at 7 Hz and 55° (fig. 8b). Similarly, at 24 hours of immersion, a resistive and capacitive behavior was described at high and middle frequencies (with a loop at 1.3 Hz and 63°, figure 8b), respectively.

At 12 and 24 hours of immersion, in both alloys a first semicircle (resistance and capacitance) is defined, indicating that it was controlled mainly by an activation process and the influence of a second semicircle attributed to the pitting and a diffusion effect on the surface. At 24 hours of immersion, the main control was due to activation at the intermediate frequencies, could suggest linear semi-infinite diffusion response or current limit at low frequencies.

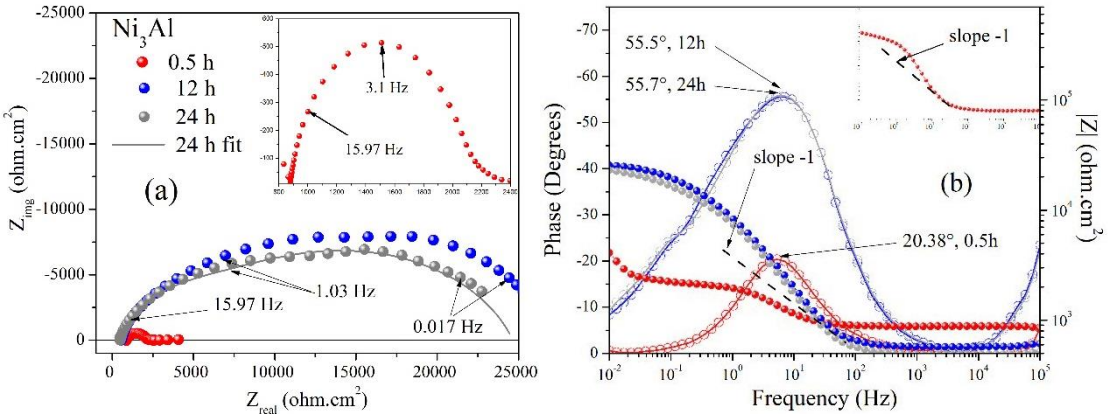

Figure 8: Electrochemistry impedance spectroscopy response for Ni_3Al, a) Nyquist and b) Bode plots in acid rain electrolyte.

Similar to Ni_3Al at 12 and 24 hours of immersion, NiAl showed a resistive behavior followed by one capacitive at high and middle frequencies, respectively; this latter describing a loop at frequencies of 1.8 Hz and 1.3 Hz to 12 and 24 hours of immersion, respectively, figure 9b. At low frequencies, at these immersion times, the behavior presented for NiAl intermetallic is similar to the intermetallic Ni_3Al, describing an activation behavior. Results of NiAl alloy showed a change in the size and shape of the diagrams, the capacitive arcs increased due to an increase in polarization resistance [23], showing a better performance in this environment as observed by the *CR*, figure 7.

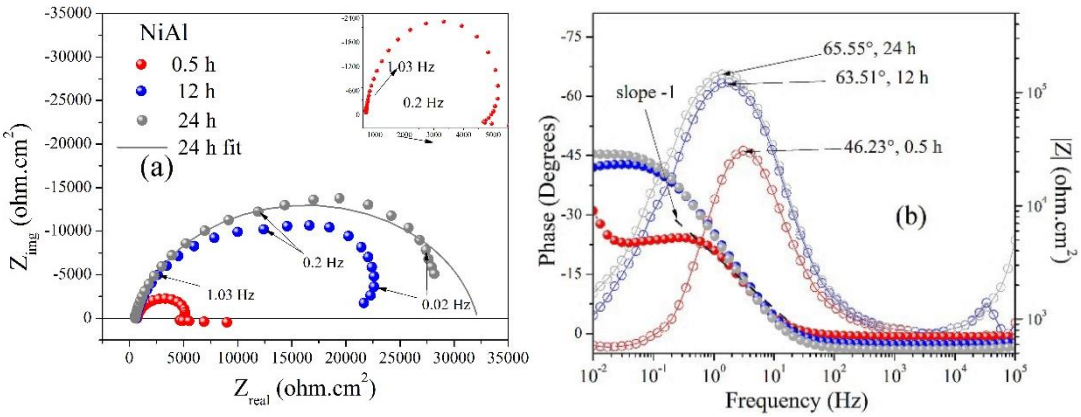

Figure 9: Electrochemistry impedance spectroscopy response for NiAl, a) Nyquist and b) Bode plots.

4. DISCUSSION

Ni_3Al characteristic microstructure consists of two phases, γ_{Ni}-γ'_{Ni3Al} corresponding to matrix and β_{NiAl}-

γ'_{Ni3Al} which corresponds to the dendritic phase. According to the phase diagram for Ni-Al, a peritectic reaction can be occur between γ-γ' and the eutectic β-γ' phases [24]. The β-γ phase is considered as metastable, this eutectic structure is formed by a rapid solidification of the samples and clearly observed at low growth rates. According to HUNZIKER and KURZ [1], the formation of the structure is thought to occur in the following sequence: growth of lamellar β-γ eutectic, nucleation of γ' in the γ phase, growth of the γ' precipitates replacing the β phase by interdiffusion of Ni and Al. From figure 6, it can be seen that the Ni_3Al-based alloy showed only localized attack (dissolution) in dendritic phases, that is, the phases with higher aluminum content. This type of preferential dissolution is observed due to the formation of micro galvanic cells, where the matrix phase acts as cathode and the dendritic phase as anode. In the presence of two phases where one of the phases has a different chemical composition or microstructure, one of these phases will act as cathode and the other as active anode; this will cause the preferential dissolution of one of the phases, which acts as an active anode, inducing a preferential and localized dissolution within the alloy [20].

According to table 3, the minor corrosion current density was presented by Ni_3Al as compared with that of NiAl, probably due to the concentrations of H_2SO_4 ($3.25x10^{-4}$ M) and HNO_3 ($2.5x10^{-4}$ M), in this sense, NiAl has a higher corrosion current density by the presence of HNO_3 for equal concentrations of H_2SO_4 and HNO_3 [9]. The anodic dissolution of both alloys may proceed via the kinetics of the anodic dissolution of Ni in acid solutions following the reaction path [25]:

$$Ni + H_2O \leftrightarrow NiOH + H^+ + e^- \quad (6$$

$$NiOH + H^+ \leftrightarrow Ni^+ + H_2O \quad (7$$

$$Ni^+ \leftrightarrow Ni^{2+} + e^- \quad (8$$

This reaction mechanism considers the water adsorption process in the mechanism of electrooxidation:

$$2H_3O^+ + 2e^- \leftrightarrow H_2O + H_2 \quad (9$$

The H_3O^+ reduction (reaction 9) is the main cathodic reaction occurring on the electrode surface.

The variation of the E_{corr} value with respect to time observed in figure 5, is a typical behavior of these alloys immersed into NaCl solution. RYBALKA K.V. *et al.* [21] have immersed a specimen of NiAl into 0.5 M NaCl solutions varying the pH, where it was observed in the solutions with pH 2.5 and 3 that the E_{corr} shifts to more negative values. In this sense, a concentration of $1.5x10^{-4}$ M NaCl was used in this work. On the other hand, the variation of the E_{corr} can be attributed to the low corrosion resistance of the Al-oxide layer in an acid medium and the difference of the Al compositions between intermetallics [24].

In the Bode plot for both intermetallics (figures 8b and 9b), the Gaussian distribution can be see in the middle frequency region a maximum in the phase angle. Whereas, it can be seen that the width of the phase angle spectrum is shifted to the high frequency region; that is, the width of the spectrum is located from the region of medium frequency to the region of high frequency, this suggests the formation of a viscous film or porous oxide on the metal surface [24]. The corrosion process of aluminum includes the formation of Al^+ ions at the metal/oxide interface, since the mobility of the Al^{3+} is low within the protective film, aluminum rapidly becomes porous Al_2O_3 on the surface of the protective film, by the following reaction:

$$2Al^{3+} + 3H_2O \leftrightarrow Al_2O_3 + 6H^- \quad (10$$

In order to interpret the electrochemical behavior of a system from EIS, an appropriate physical model

of the electrochemical reactions occurring at the electrode surface is necessary, figure 10. For the Ni_3Al alloy, R_s is the solution resistance, CPE_{dl} the double layer capacitance and R_{ct} charge transfer resistance by roughness effect, CPE_1 and R_1 are the capacitance and resistance of the diffusive and localized corrosion processes occurring on the metal surface. While for NiAl alloy, the elements are Rs electrolyte resistance, CPE_{dl} double layer capacitance and R_{ct} charge transfer resistance. The values obtained by Zview2 software from the circuits are reported in Table 4.

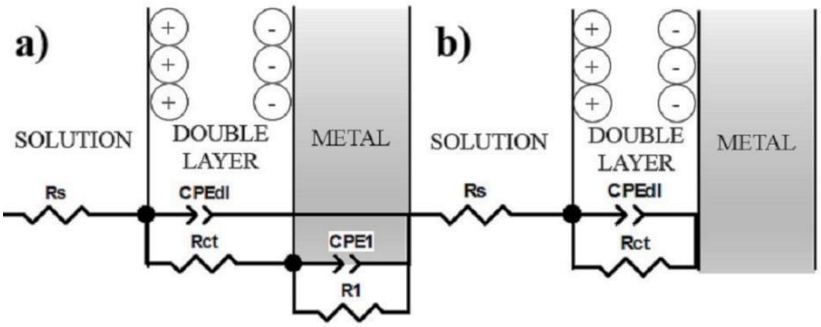

Figure 10: Equivalent electrics circuits used to simulate the EIS data of, a) Ni_3Al and b) NiAl alloys.

Table 5: Fitting parameters used to simulate the EIS data of Ni_3Al and NiAl alloys in simulated acid rain.

SAMPLES	R_s (Ωcm^2)	C_{dl} (F/cm^2)	R_p (Ωcm^2)	CPE (F/cm^2)	R (Ωcm^2)
NiAl	536.4±1.15%	$3.797x10^{-5}$±2.43%	31621±2.35%	------	------
Ni_3Al	473±1.63%	$1.553x10^{-5}$±4.02%	9205±2.74%	$8.359x10^{-5}$±1.55%	15000±9.26%

5. CONCLUSIONS

From the current results obtained in this research work, it can be concluded the following:

- The Ni_3Al-based alloy showed only localized attack (dissolution) in dendritic phases, its type of preferential dissolution is observed due to the formation of micro galvanic cells.
- NiAl have a higher corrosion current density in the presence of HNO_3 for equal concentrations of H_2SO_4 and HNO_3.
- The variation of the E_{corr} can be attributed to the low corrosion resistance of the Al-oxide layer in an acid medium and the difference of the Al composition between intermetallics.
- The width of the phase angle spectrum is shifted to the high frequency region due to the formation of a porous oxide.

6. ACKNOWLEDGMENTS

Engelbert Huape thanks to the CONACYT of the grant to carry out his doctoral studies and the memory of Ph.D. Alberto Martinez Villafañe

7. BIBLIOGRAPHY

[1] HUNZIKER O. and KURZ W. "Solidification microstructure maps in ni-al alloys", *Acta mater*, v. 45, n. 12, pp. 4981-4992, 1997.

[2] ALBITER A., *et al*. "Corrosion performance of NiAl intermetallic with Mo, Ga and Fe in neutral and alkaline media". *Journal of Applied Electrochemistry*, v. 34, pp. 1141–1145, 2004.

[3] GUO J.T., *et al.*, "Microstructure and mechanical properties of Ni_3Al and Ni_3Al-1B alloys fabricated by SHS/HE". *Intermetallics*, v. 19, pp. 137-142, 2011.

[4] SCHWEIGER H., *et al.*, "Energetics of point defect formation in Ni_3Al", *Scripta Materialia*, v. 46, pp. 37-41, 2002.

[5] ZHAO H.L., *et al.*, "Effect of different strain rates on compression property and work-hardening behavior for the NiAl-matrix composite with 1.7 wt.% NbB_2 and Nb_xC*"*, *Materials Science and Engineering*, v. A534,

pp. 22– 25, 2012.

[6] ZHOU J. and GUO J., "Effect of Ag alloying on microstructure, mechanical and electrical properties of NiAl intermetallic compound", *Materials Science and Engineering*, v. A339, pp. 166-174, 2003.

[7] SHIOMI S., *et al.*, "Aluminide Coatings Fabricated on Nickel by Aluminium Electrodeposition from DMSO2-Based Electrolyte and Subsequent Annealing", *Materials Transactions*, v. 52, n. 6, pp. 1216-1221, 2011.

[8] JIAN-HONG LIAO, *et al.*, "Influence of Rhenium on the Grain Boundary Strength, Phase Evolution, and High Temperature Mechanical Properties of a Fine-Grain Nickel-Base Superalloy at 982°C", *Materials Transactions*, v. 52, n. 10, pp. 1989-1997, 2011.

[9] ALBITER A., *et al.*, "Effect of Mo, Ga and Fe on the corrosion resistance of nanocrystalline NiAl alloy in acidic media", *International Journal of Hydrogen Energy*, v. 30, pp. 1311-1315, 2005.

[10] CASTAÑEDA I.E., *et al.*, "Corrosion Behavior of Ni-Al-Cu Alloys in Simulated Human Body Solution". *Int. J. Electrochem. Sci*., v. 6, n. 2, pp. 404-418, 2011.

[11] TRINSTANCHO-REYES J.L. *et al*. "Electrochemical Impedance Spectroscopy Investigation of Alloy Inconel 718 in Molten Salts at High Temperature", *Int. J. Electrochem. Sci*., v. 6, n. 2, pp. 419-431, 2011.

[12] EN-U LIU and CHIUNG-PIN LIU, "Effects of Simulated Acid Rain on the Antioxidative System in Cinnamomum philippinense Seedlings", *Water Air Soil Pollut*, v. 215, n. 1, pp. 127-135, February 2011.

[13] WANG H. and HAN G., "Chemical composition of rainwater and anthropogenic influences in Chengdu, Southwest China", *Atmospheric Research*, v. 99, pp. 190–196, 2011.

[14] PATRÍCIA S.M., *et al*., "Chemical composition of rainwater at a coastal town on the southwest of Europe: What changes in 20 years?". *Science of the Total Environment*, v. 409, pp. 3548–3553, 2011.

[15] YANG L., *et al*., "Corrosion behaviour of superplastic Zn–Al alloys in simulated acid rain", *Corrosion Science*, v. 59, pp. 229–237, 2012.

[16] LUCCA D.A., *et al.*, "Nanoindentation: Measuring methods and applications", *CIRP Annals - Manufacturing Technology*, v. 59, pp. 803–819, 2010.

[17] OLIVER W.C. and PHARR G.M., "An improved technique for determining hardness and elastic modulus using load and displacement sensing indentation experiments", *J. Mater. Res.*, v. 7, n. 6, pp. 1564-1583, Jun 1992.

[18] FENG L. *et al.*," Corrosion behavior of AZ31 magnesium alloy in simulated acid rain solution", *Trans. Nonferrous Met. Soc. China*, v. 20, pp. s638−s642, 2010.

[19] SHI D., et al., "First-principles studies of Al–Ni intermetallic compounds". *Journal of Solid State Chemistry*, v. 182, pp. 2664–2669, 2009.

[20] GONZALEZ-RODRIGUEZ J.G., *et al.*, "Effect of macroalloying with Cu on the corrosion resistance of rapidly solidified NiAl intermetallic in 0.5 M H2SO4", *Materials Science and Engineering*, v. A448, pp. 158–164, 2007.

[21] RYBALKA K.V., *et al*.," Electrochemical behavior and the rate of general corrosion of NiAl intermetallic compound in the unbuffered sodium chloride solutions". *Corrosion Science*, v. 53, pp. 630–636, 2011.

[22] MOHAMMED A., *et al*., "Electrochemical and Corrosion Behavior of cast Re-containing Inconel 718 Alloys in Sulphuric Acid Solutions and the Effect of Cl", *Int. J. Electrochem. Sci*., v. 9, n. 9, pp. 5352 – 5374, September 2014

[23] NELSY RAGUÁ C., *et al.*, "Erosión - corrosión de un acero aisi sae 1020 en un sistema salmuera-co2-arena", *Scientia et Technica*, v. 35, n. 213, August 2007.

[24] PORCAYO-CALDERON J., *et al*., "Effect of Cu Addition on the Electrochemical Corrosion Performance of Ni3Al in 1.0M H2SO4", *Advances in Materials Science and Engineering*, v. 2015, November 2015.

[25] EL-BAGOURY N., et al. "Effect of Various Heat Treatment Conditions on Microstructure, Mechanical Properties and Corrosion Behavior of Ni Base Superalloys", *Int. J. Electrochem. Sci*., v. 6, pp. 6718 – 6732, 2011.